DOI: 10.19884/j.1672-5220.202404008

Piezo-Photocatalytic Technology Based on Bismuth Ferrite ($Bi_2Fe_4O_9$) for Degradation of Reactive Dye KN-R

ZHU Feishi[1,2], HU Chunyan[1,2], LIU Baojiang[1,2*]

1. Key Laboratory of Science and Technology of Eco-Textile, Ministry of Education, Donghua University, Shanghai 201620, China
2. College of Chemistry and Chemical Engineering, Donghua University, Shanghai 201620, China

Abstract: Dyeing wastewater poses a serious threat to environmental protection and industrial development. The piezoelectric effect can be used to optimize the band structure of semiconductors and improve the photon efficiency of photocatalysts. $Bi_2Fe_4O_9$, a narrow gap semiconductor with piezoelectric effect, was prepared by a hydrothermal synthesis method for the degradation of reactive dye KN-R. The results show that the degradation efficiency of KN-R can be significantly improved by piezo-photocatalysis, and the degradation rate constant of piezo-photocatalysis $k_{pi\text{-}ph}$ is about 3.4 times as large as the degradation rate constant of piezoelectric catalysis k_{pi} and about 2.6 times as large as the degradation rate constant of photocatalysis k_{ph}. At a pH value of 3 and a lower KN-R mass concentration (60 mg/L), a higher degradation efficiency (98.5%) is achieved. CO_3^{2-} and cationic surfactant (CTAB) inhibit the degradation of KN-R. It is proved that the contributions of different active species to the degradation of KN-R follow the order: $\cdot OH$, $\cdot O_2^-$, h^+, and $^1O_2$. The possible mechanism of piezo-photocatalytic degradation of KN-R was discussed. The photoexcitation generates a large amount of free charges, and the piezoelectric effect modulates the energy band structure of $Bi_2Fe_4O_9$ and promotes the separation of photogenerated electron-hole pairs. The synergistic effect of the two factors significantly improves the degradation efficiency of KN-R.

Keywords: $Bi_2Fe_4O_9$; piezo-photocatalysis; degradation; wastewater treatment; reactive dye KN-R

CLC number: X52 **Document code**: A

Article ID: 1672-5220(2025)01-0001-11

Open Science Identity
(OSID)

0 Introduction

Water pollution has significant negative impacts on human health, socio-economic development and ecological environment. Globally, a large amount of organic dye wastewater is discharged annually, which leads to an increasing concentration of organic dyes in water bodies and serious pollution of the water environment[1]. To address these challenges, there is an urgent need to develop new, efficient and environmentally friendly water treatment technologies for wastewater. Photocatalytic degradation of pollutants is a promising approach due to its greenness, efficiency and simplicity[2-3]. However, the activity of photocatalysts is significantly impacted by photon yield and electron-hole separation efficiency. Improving the photon yield and carrier separation rate of photocatalysts is currently a significant research topic[4-6].

Piezoelectric materials generate piezoelectric potentials in response to mechanical vibrations. Built-in piezoelectric electric fields are considered to be an effective strategy to enhance photogenerated carrier separation and transport[7-12]. Researchers[13-14] presented the piezoelectric electrochemical effects of ZnO microfibers and $BaTiO_3$ microcrystals on water cracking and dye degradation under ultrasonic vibration. Numerous research experiments have shown that piezoelectric semiconductor materials affect the energy band structure of photoelectron-hole pairs and the separation of photoelectron-hole pairs by generating an internal electric field under external vibration conditions[15-17].

$Bi_2Fe_4O_9$ is composed of alternating layers of bismuth-oxygen (Bi—O hexahedral) and iron-oxygen (Fe—O octahedral and Fe—O tetrahedral). Related studies have shown that there is spontaneous polarization within the $Bi_2Fe_4O_9$ crystal, where the $6s^2$ lone electron pair on Bi^{3+} hybridizes with the 2p orbital of O^{2-}, leading to the symmetry breaking of $Bi_2Fe_4O_9$, which gives rise to piezoelectric effects[18-19]. $Bi_2Fe_4O_9$ is also a narrow bandgap semiconductor with a bandgap width around 2.0 eV and has a wide response range in the visible spectrum[20-21]. $Bi_2Fe_4O_9$ is a non-toxic, low-cost, recyclable and chemically stable bismuth-based light-driven material. $Bi_2Fe_4O_9$ can be prepared by solid-phase, sol-gel and hydrothermal methods. In view of the piezoelectric effect, excellent photocatalytic performance,

---

Received date: 2024-04-12

* Correspondence should be addressed to LIU Baojiang, email: bjliu@dhu.edu.cn

Citation: ZHU F S, HU C Y, LIU B J. Piezo-photocatalytic technology based on bismuth ferrite ($Bi_2Fe_4O_9$) for degradation of reactive dye KN-R[J]. *Journal of Donghua University (English Edition)*, 2025, 42(1): 1-11.

low cost, environmental friendliness and high stability, $Bi_2Fe_4O_9$ has received wide attention in the fields of photocatalysis[22-23], piezoelectric catalysis[24-25] and active oxidants[26-27].

Therefore, in this research, photocatalyst $Bi_2Fe_4O_9$ nanosheets with the piezoelectric effect were synthesized to degrade dye wastewater simulated by reactive dye KN-R. Photocatalytic, piezoelectric and piezo-photocatalytic degradation performances of the synthesized $Bi_2Fe_4O_9$ were compared. The effects of pH values, common ions and surfactants on the degradation efficiency were discussed, and major active species were verified by the electron spin resonance (ESR) test and quenching experiments. The possible piezo-photocatalytic degradation mechanism was discussed.

1 Materials and Methods

1.1 Materials

All the reagents were analytical grade and used directly without further purification. Bismuth nitrate hydrate ($Bi(NO_3)_3 \cdot 5H_2O$), ferric nitrate hydrate ($Fe(NO_3)_3 \cdot 9H_2O$), nitric acid (HNO_3), hydrochloric acid (HCl), sodium hydroxide (NaOH), methyl alcohol (CH_3OH), ethyl alcohol (C_2H_5OH), *p*-benzoquinone (*p*-BQ), tert-butanol (*t*-BuOH), furfuryl alcohol (FFA), sodium oxalate (AO-Na), 5,5-dimethyl-1-pyrroline N-oxide (DMPO), 2,2,6,6-tetramethyl-4-piperidone (TEMP), sodium chloride (NaCl), sodium sulfate (Na_2SO_4), sodium carbonate (Na_2CO_3), calcium chloride ($CaCl_2$) and magnesium chloride ($MgCl_2$) were purchased from Sinopharm Chemical Reagent Co., Ltd. (Shanghai, China). Reactive dye KN-R (KN-R in short), polyethylene glycol 2000 (PEG-2000), sodium dodecyl sulfate (SDS) and cetyltrimethyl ammonium bromide (CTAB) were obtained from Aladdin Chemical Co., Ltd. (Shanghai, China). The deionized water was used throughout the experiments.

1.2 Synthesis of $Bi_2Fe_4O_9$

$Bi_2Fe_4O_9$ was synthesized utilizing a hydrothermal method that was adapted from Refs. [28 – 30], with further modifications to optimize the synthesis process. $Bi(NO_3)_3 \cdot 5H_2O$ and $Fe(NO_3)_3 \cdot 9H_2O$ were dissolved in 0.4 mol/L concentrated HNO_3 (80 mL) at a molar ratio of 1 : 2. Solid NaOH was added to the solution to maintain a concentration of 12 mol/L, and the mixture was stirred thoroughly for 0.5 h. Subsequently, the precursor was transferred to a 100 mL polytetrafluoroethylene reaction liner and reacted at 190 ℃ for 12 h in a high-temperature and high-pressure reactor. It was then cooled overnight and washed three times with dilute HNO_3, deionized water and C_2H_5OH, respectively. Finally, it was dried at 60 ℃. The systhesis diagram of $Bi_2Fe_4O_9$ is shown in Fig. 1.

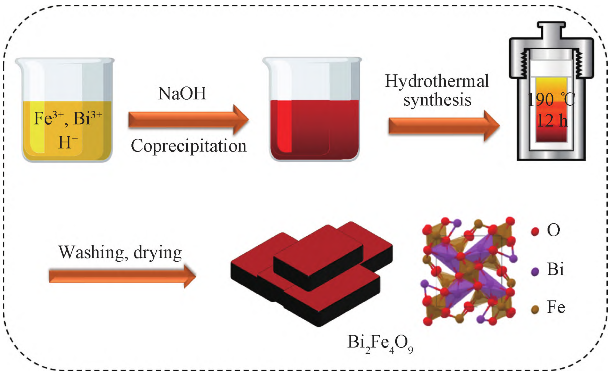

Fig. 1 Systhesis diagram of $Bi_2Fe_4O_9$

1.3 Characterization of $Bi_2Fe_4O_9$

The crystalline structure of $Bi_2Fe_4O_9$ was characterized by X-ray diffraction (XRD) (D/Max-2550PC, Rigaku Corporation, Japan). The elemental compositions and chemical states of $Bi_2Fe_4O_9$ were analyzed by X-ray photoelectron spectroscopy (XPS) (AXIS Supra, Shimadzu Corporation, Japan). The microscopic morphology of $Bi_2Fe_4O_9$ was characterized by scanning electron microscopy (SEM) (JSM-5600LV, JEOL Ltd., Japan). The ultramicroscopic morphology and lattice resolution of $Bi_2Fe_4O_9$ were characterized by transmission electron microscopy (TEM) (Talos F200S, FEI Co., the Netherlands). The light absorption properties of $Bi_2Fe_4O_9$ were tested by ultraviolet-visible diffuse reflectance spectroscopy (UV-Vis DRS) (Shimadzu UV-3600, Shimadzu Corporation, Japan). The active species of $Bi_2Fe_4O_9$ were detected by an ESR instrument (JEOL-FA200, JEOL Ltd., Japan). The piezoelectric properties of $Bi_2Fe_4O_9$ were tested by piezoelectric force microscopy (PFM) (Dimension Icon, Bruker (Beijing) Scientific Technology Co., Ltd., China).

1.4 Experimental process

In this study, KN-R was used as the degradation substrate, the ultrasonic cleaner (40 kHz, 600 W) (SK3200HP, Shanghai Kudos Ultrasonic Instrument Co., Ltd., China) was used as the mechanical pressure device, and the Xe lamp (300 W, $\lambda > 400$ nm) (BL-GHX-V, Shanghai Biron Instrument Co., Ltd., China) was used as the simulated light source. The piezo-photocatalytic activity of $Bi_2Fe_4O_9$ was evaluated under ultrasonic and visible light irradiation. First, $Bi_2Fe_4O_9$ (30 mg, 0.6 g/L) was dispersed into KN-R solution (50 mL), and the reaction was carried out for 60 min under the ultrasonic and visible light environment. Every 10 min, 3 mL of the supernatant was collected and filtered through a 0.22 μm filter, and then the absorbance of the filtered solution at the maximum absorption wavelength (590 nm) was measured by UV-Vis DRS. The kinetic rate of KN-R degradation is calculated as

$$\ln\left(\frac{C_r}{C_0}\right)=-kt, \qquad (1)$$

where C_0 and C_r are the initial concentration and residual concentration of KN-R, respectively; k is the first-order kinetic rate constant; t indicates the reaction time.

2 Results and Discussion

2.1 Characterization of $Bi_2Fe_4O_9$

Figure 2(a) shows the XRD pattern of $Bi_2Fe_4O_9$, with the inset providing a detailed view of the standard diffraction pattern of $Bi_2Fe_4O_9$ (Joint Committee on Powder Diffraction Standard, JCPD # 25-0090). The diffraction peaks of 14.7°, 28.1°, 28.8°, 33.6° and 47.0° correspond to the (001), (121), (211), (130) and (141) crystal faces of $Bi_2Fe_4O_9$, respectively, indicating that the $Bi_2Fe_4O_9$ crystal has been synthesized successfully. Figures 2(b) and 2(d) present SEM and TEM images of $Bi_2Fe_4O_9$, which more intuitively reveal that $Bi_2Fe_4O_9$ exhibits a square shape. Figure 2(c) shows that the average size of $Bi_2Fe_4O_9$ is (329.44 ± 130.38) nm. Figure 2(e) shows the high-resolution TEM (HRTEM) image of $Bi_2Fe_4O_9$, and the lattice spacing d of $Bi_2Fe_4O_9$ is about 0.266 nm, corresponding to the (130) crystal face of the mullite phase $Bi_2Fe_4O_9$. The XPS survey spectrum of $Bi_2Fe_4O_9$ is shown in Fig. 2(f). Figure 2(g) shows the XPS spectrum of Bi 4f[31]. The peaks of 164.2 eV and 159.0 eV represent the $4f_{5/2}$ and $4f_{7/2}$ orbitals of the Bi element, respectively. Figure 2(h) shows the characteristic peaks of the Fe element in the 2p orbit, with Fe $2p_{3/2}$ and Fe $2p_{1/2}$ corresponding to peaks at 711.0 eV and 724.0 eV, respectively. The peaks at binding energies of 725.1 eV and 711.4 eV correspond to Fe(III), and those at binding energies of 722.8 eV and 709.4 eV correspond to Fe(II). The remaining characteristic peaks are satellite peaks of Fe(III) and Fe(II)[32-33]. Figure 2(i) shows the characteristic peaks of O 1s, where 529.5 eV corresponds to lattice oxygen (O_L) and 531.8 eV corresponds to adsorbed oxygen (O_C). The adsorbed oxygen can obtain superoxide radicals that capture the electrons generating active species on the surface of $Bi_2Fe_4O_9$ and plays an important role in the catalytic process[34-35].

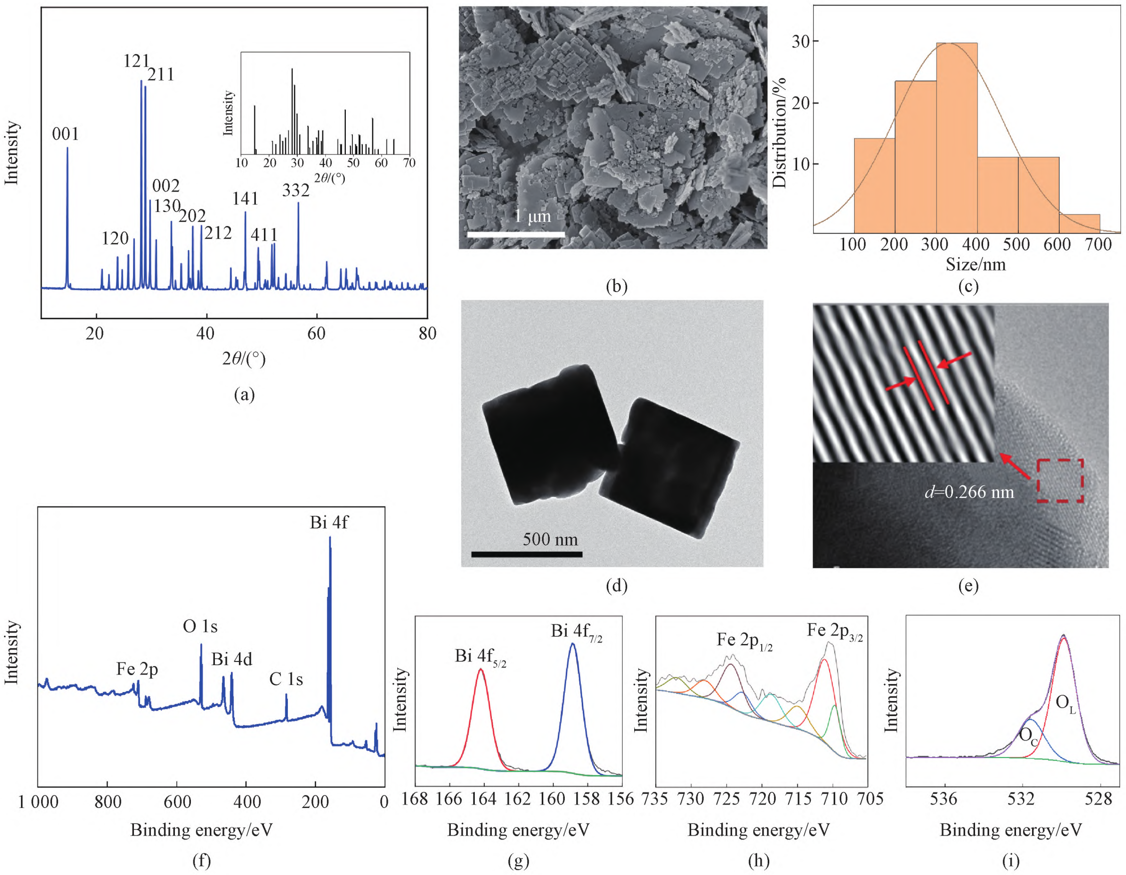

(a) (b) (c) (d) (e) (f) (g) (h) (i)

Fig. 2 Characterization of $Bi_2Fe_4O_9$: (a) XRD pattern; (b) SEM image; (c) size distribution; (d) TEM image; (e) HRTEM image; (f) XPS survey spectrum; (g) XPS spectrum of Bi 4f; (h) XPS spectrum of Fe 2p; (i) XPS spectrum of O 1s

Figure 3(a) shows typical butterfly loops observed under the application of an applied electric field, with a maximum amplitude of about 145 pm. Figure 3(b) shows the hysteresis loops of $Bi_2Fe_4O_9$. When the applied forward voltage is 10 V, the phase value is about 50°; when the voltage changes to −10 V, the phase value is nearly −130°. The absolute phase value of the positive and negative turnover difference of the domain structure within the crystal is about 180°. It indicates that the domain structure is flipped in the opposite direction in the lattice, which proves the piezoelectric effect of $Bi_2Fe_4O_9$. In addition, PFM can also be used to characterize the surface topography of $Bi_2Fe_4O_9$. Figure 3(c) shows the three-dimensional (3D) morphological image of $Bi_2Fe_4O_9$, Fig. 3(d) is the amplitude image, and Fig. 3(e) is the phase image in which the light and dark regions indicate different polarization directions[36].

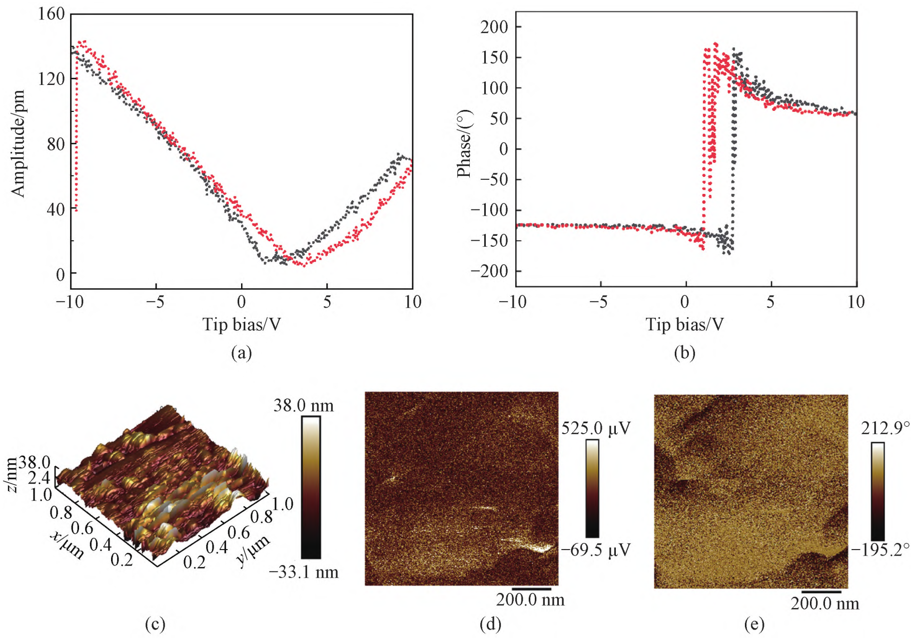

(a) (b)

(c) (d) (e)

Fig. 3 PFM analyses of $Bi_2Fe_4O_9$: (a) piezoelectric butterfly loops; (b) hysteresis loops; (c) 3D morphological image; (d) amplitude image; (e) phase image

2.2 Performance of piezo-photocatalysis

Figure 4(a) shows the effects of photocatalytic (under the light condition, denoted as UL), piezoelectric catalytic (under the ultrasonic condition, denoted as US) and piezo-photocatalytic (under both ultrasonic and light conditions, denoted as US/UL) degradation of KN-R by $Bi_2Fe_4O_9$, respectively. The experiment is conducted under the following conditions: the dosage of $Bi_2Fe_4O_9$ is 30 mg, the volume of 100 mg/L KN-R is 50 mL, the pH value is 3, and the temperature is 25 ℃. The inset in Fig. 4(a) shows the color change of KN-R solution at 0, 20, 40 and 60 min of piezo-photocatalysis. Under dark and non-ultrasonic conditions, the adsorption efficiency of $Bi_2Fe_4O_9$ on KN-R is about 20.0%, the degradation efficiency of the single photocatalysis is close to 50.0%, the degradation efficiency of the single piezoelectric catalysis is about 65.0%, and the degradation efficiency of ultrasonic and light combined piezo-photocatalysis is about 70.8%, which suggests that the degradation efficiency is significantly improved. Figure 4(b) shows the kinetic fitting diagram. The first-order kinetic rate constant values of piezoelectric catalysis, photocatalysis and piezo-photocatalysis are $k_{\rm pi} = 0.005\,08\ \mathrm{min}^{-1}$, $k_{\rm ph} = 0.006\,73\ \mathrm{min}^{-1}$ and $k_{\rm pi\text{-}ph} = 0.017\,20\ \mathrm{min}^{-1}$, respectively. It means that $k_{\rm pi\text{-}ph}$ is about 3.4 times as large as $k_{\rm pi}$ and about 2.6 times as large as $k_{\rm ph}$. Figure 4(c) shows the instantaneous response currents under UL, US and US/UL conditions. Compared with the current under the UL or US condition, the current under the US/UL condition shows a significantly stronger amplitude, confirming the synergistic effect between piezoelectricity and light.

Figure 5 shows the piezo-photocatalytic degradation efficiency of KN-R at different pH values. The pH value range is set between 1 and 11 because KN-R can be hydrolyzed when the alkalinity is too strong. Other experimental conditions are as follows: the dosage of $Bi_2Fe_4O_9$ is 30 mg, the volume of 100 mg/L KN-R is 50 mL and the temperature is 25 ℃. The results show that under alkaline and neutral conditions, $Bi_2Fe_4O_9$ exhibits little piezo-photocatalytic effect on the degradation of KN-R. However, with the decrease of pH value, the catalytic effect is significantly enhanced. When the pH value is 3, the catalytic effect is the best. As the pH value continues to decrease, the catalytic performance becomes slightly less effective. KN-R, as an anionic dye, has a negative surface charge under neutral or alkaline conditions, and there is a repulsive effect with the negatively charged $Bi_2Fe_4O_9$, and thus the catalytic effect of $Bi_2Fe_4O_9$ is reduced. Under certain acidic conditions, the hydroxyl group on the surface of $Bi_2Fe_4O_9$ is more easily combined with H^+ to generate hydroxyl radical, which enhances the catalytic effect. As the protonation degree of KN-R increases, it becomes more susceptible to adsorption and degradation by $Bi_2Fe_4O_9$.

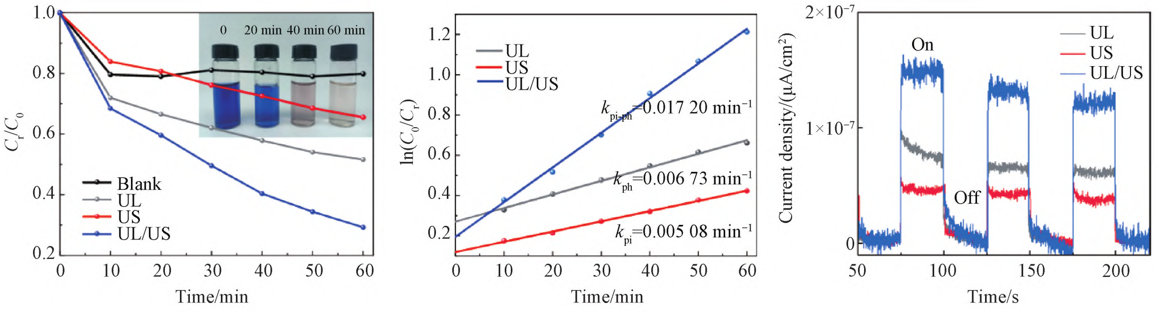

(a) (b) (c)

Fig. 4 Photocatalysis, piezoelectric catalysis and piezo-photocatalysis: (a) KN-R degradation efficiencies; (b) rate constants; (c) instantaneous response currents

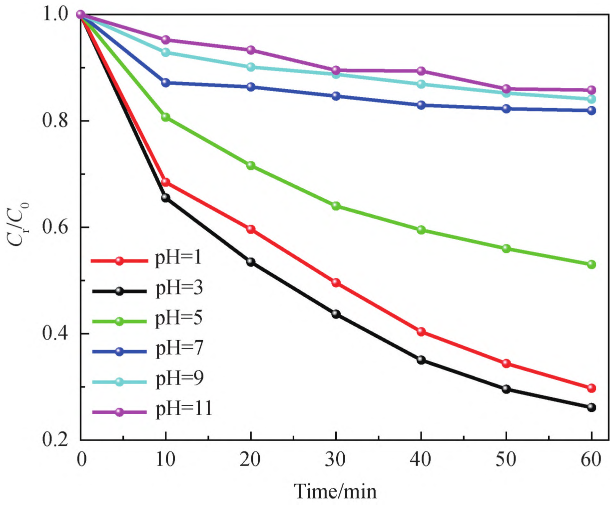

Fig. 5 Effect of pH on degradation of KN-R

Figure 6 shows the influences of different factors on the degradation efficiency and recycling effect. The experiment is conducted under the following conditions: the dosage of $Bi_2Fe_4O_9$ is 30 mg, the pH value is 3 and the temperature is 25 ℃. Figure 6(a) shows the piezo-photocatalytic degradation efficiency at different mass concentrations (60, 100 and 140 mg/L) of degradation substrate KN-R. The degradation efficiencies are 80.9% (60 mg/L), 51.2% (100 mg/L) and 49.1% (140 mg/L) at 30 min and 98.5% (60 mg/L), 70.0% (100 mg/L) and 61.1% (140 mg/L) at 60 min, respectively. When the mass concentration of KN-R increases, on the one hand, the absorption of visible light by $Bi_2Fe_4O_9$ decreases; on the other hand, the limitation of the active sites on the surface of $Bi_2Fe_4O_9$ leads to the decrease of the degradation efficiency.

Inorganic salts (e.g. Na_2SO_4) are used in large quantities in the dyeing and printing process. To investigate the effect of common inorganic salt ions on the degradation efficiency, five KN-R solutions containing NaCl, Na_2SO_4, Na_2CO_3, $CaCl_2$ and $MgCl_2$, respectively, with a concentration of 20 mmol/L are prepared. Figure 6(b) shows that all inorganic salt ions except Na^+ inhibit the degradation efficiency of KN-R to some extent, and the inhibition effect of Cl^-, Ca^{2+} and Mg^{2+} is weak, while the inhibition effect of SO_4^{2-} and CO_3^{2-} is very strong. The KN-R degradation efficiency decreases from 98.5% to 72.4% under the influence of SO_4^{2-} and decreases from 98.5% to 53.4% under the influence of CO_3^{2-}. Surfactants are also widely used in the dyeing and printing process. To investigate the effect of surfactants on the piezo-photocatalytic degradation of KN-R by $Bi_2Fe_4O_9$, three KN-R solutions containing anionic surfactant SDS, cationic surfactant CTAB and nonionic surfactant PEG-2000, respectively, with a concentration of 20 mmol/L are prepared. Figure 6(c) shows that the nonionic surfactant PEG-2000 has no significant effect on the degradation of KN-R; the degradation efficiency of KN-R is partially inhibited by the anionic surfactant SDS, and the degradation efficiency decreases from 98.0% to 75.0%. The cationic surfactant CTAB has a strong inhibitory effect on the degradation of KN-R, and the degradation efficiency decreases from 98.5% to 53.4%.

Figure 6 (d) shows the piezo-photocatalytic degradation efficiency of different kinds of dyes at the pH value of 3. Four different kinds of dyes are selected for the experiment: KN-R, anionic dye methyl orange (MO), cationic dye methylene blue (MB) and nonionic dye disperse blue 56 (E-4R). The mass concentration of the dye is 60 mg/L. The highest degradation efficiency is achieved for anionic dyes (98.5% for KN-R and 96.9% for MO), followed by nonionic dye (92.3% for E-4R), and the lowest degradation efficiency is achieved for the cationic dye (75.7% for MB). $Bi_2Fe_4O_9$ can be recycled from the degradation solution by filtration, washing and drying. Figure 6(e) demonstrates the degradation efficiency of five cycling experiments, and the degradation efficiency remains high at 88.9% after five cycles. Figure 6(f) proves that the structure of $Bi_2Fe_4O_9$ is stable after five cycles without shifts and stray peaks. In Fig. 6(f), fresh represents the $Bi_2Fe_4O_9$ sample before the recycling degradation experiment and used represents the sample after the recycling degradation experiment.

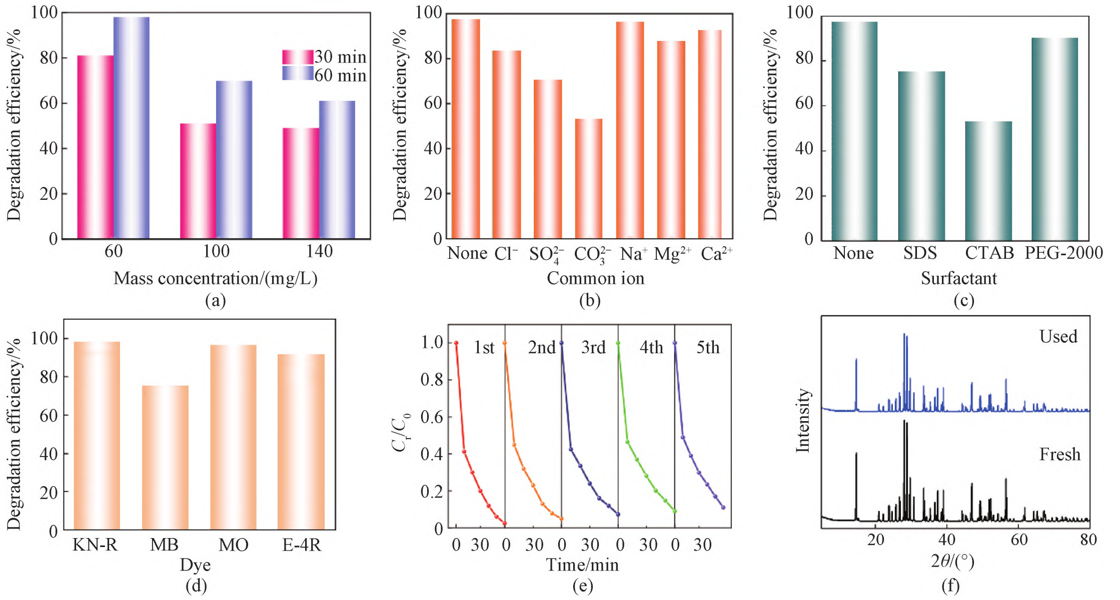

Fig. 6 Influences on degradation efficiency and recycling effect: (a) KN-R mass concentrations; (b) common ions; (c) surfactants; (d) different dyes; (e) recycling effect; (f) XRD patterns

2.3 Identification of active species

To investigate the major active species during piezo-photocatalysis, AO-Na, *p*-BQ, *t*-BuOH and FFA are added to the KN-R solution as quenchers for hole (h^+), superoxide free radical ($\cdot O_2^-$), hydroxyl free radical ($\cdot OH$) and monomer oxygen ($^1O_2$), respectively. As shown in Fig. 7(a), the degradation efficiency of KN-R with AO-Na, *p*-BQ, *t*-BuOH and FFA decreases from 98.5% (no quencher) to 50.3%, 42.8%, 33.9% and 85.1%, respectively. Therefore, it can be concluded that the contributions of different active species to the degradation of KN-R follow the order: $\cdot OH$, $\cdot O_2^-$, h^+, and $^1O_2$.

ESR is used for the identification of active species. The test results are shown in Figs. 7(b)–7(d). In Fig. 7(b), the peak signal of DMPO-$\cdot O_2^-$ is detected under both UL and US conditions, and the peak signal of DMPO-$\cdot O_2^-$ is further enhanced under the US/UL condition. As shown in Fig. 7(c), no obvious TEMP-$^1O_2$ peak signal is detected under the condition of UL alone, while a weak TEMP-$^1O_2$ peak signal is detected under the condition of US alone. However, the peak signal of TEMP-$^1O_2$ increases significantly under the condition of US/UL. Similarly, in Fig. 7(d), no DMPO-$\cdot OH$ peak signal is detected under the condition of UL alone, while a weak DMPO-$\cdot OH$ peak signal is detected under the condition of US alone, and the peak signal is enhanced when US and UL are combined. The above experimental results show that the synergistic effect of ultrasonic and light significantly enhances the active species generated on $Bi_2Fe_4O_9$ surface.

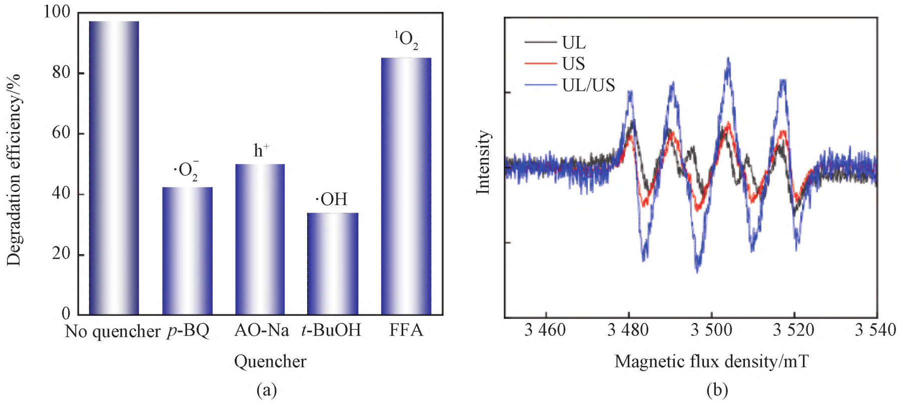

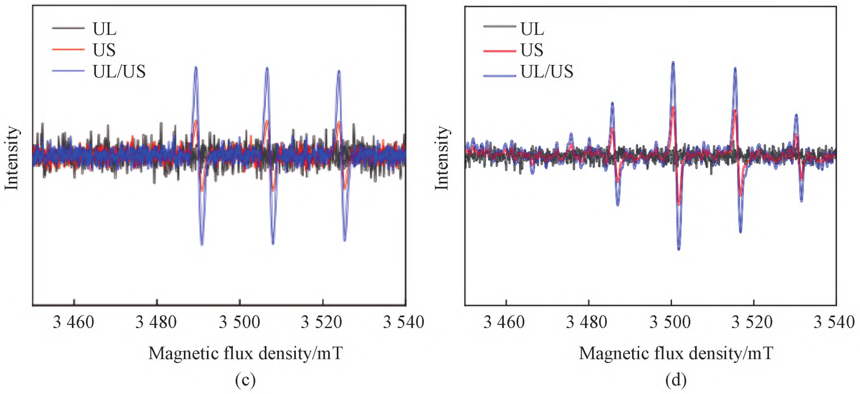

(c) (d)

Fig. 7 Analyses of active species: (a) effect of quencher on degradation efficiency; (b) DMPO-$\cdot O_2^-$; (c) TEMP-$^1O_2$; (d) DMPO-·OH

2.4 Mechanism of piezo-photocatalysis

The UV-Vis DRS test can be used to characterize the absorption performance of the solar spectrum. As shown in Fig. 8(a), $Bi_2Fe_4O_9$ has a strong absorption performance in the visible region below 600 nm, and a weak absorption performance in the visible region above 600 nm. In addition, according to the Kubelka-Munk function equation, the measurement data of UV-Vis DRS spectrum can be converted into a curve of $h\nu$-$(\alpha h\nu)^2$ (shown in the inset of Fig. 8(a)), where $h\nu$ is the photon energy and α is the absorbance at the corresponding wavelength. The bandgap width of $Bi_2Fe_4O_9$ can be calculated according to this curve. According to the extrapolation of the linear part of the curve and the x-axis intercept, the bandgap test result of the material can be obtained[37-38]. It can be seen from Fig. 8(a) that the bandgap value E_g of $Bi_2Fe_4O_9$ is about 2.16 eV.

To determine the band of $Bi_2Fe_4O_9$, the Mott-Schottky curve is tested to estimate its flat-band potential. The Mott-Schottky curve of $Bi_2Fe_4O_9$ is shown in Fig. 8(b), where C represents capacitance. The intersection point between the tangent line of the Mott-Schottky curve and the x-axis is the corresponding flat-band potential[39]. It can be obtained that the flat-band potential E_{fb} of $Bi_2Fe_4O_9$ is −0.63 eV (vs. Ag/AgCl). In this research, the Mott-Schottky test electrolyte is Na_2SO_4 solution, with a pH value of 6.8. Therefore, the relative standard hydrogen potential (NHE) can be calculated as

$$E_{CB} = E_{fb} + 0.197, \tag{2}$$

$$E_{VB} = E_g + E_{CB}. \tag{3}$$

According to Eq. (2), the conduction band (CB) potential E_{CB} of $Bi_2Fe_4O_9$ is estimated to be −0.43 eV. According to Eq. (3), the valence band (VB) potential E_{VB} of $Bi_2Fe_4O_9$ is estimated to be 1.73 eV.

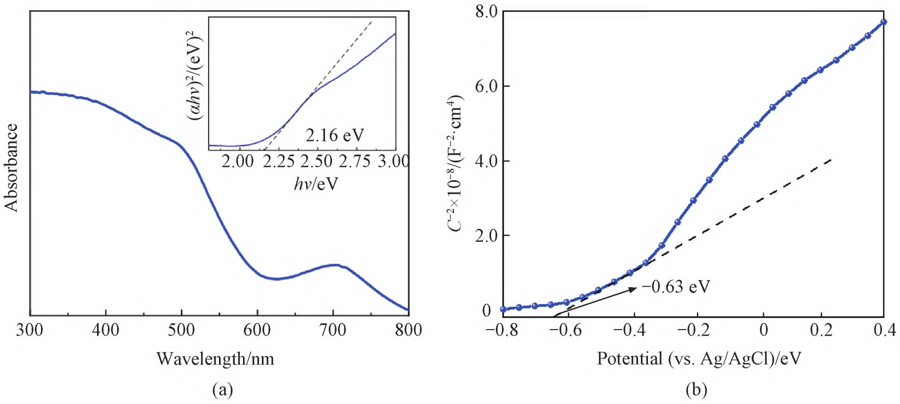

(a) (b)

Fig. 8 Optical properties of $Bi_2Fe_4O_9$: (a) UV-Vis DRS spectrum and $(\alpha h\nu)^2$-$(h\nu)$ curve; (b) Mott-Schottky curve

Based on the above analyses, we propose the possible mechanism of piezo-photocatalytic degradation of KN-R by $Bi_2Fe_4O_9$. The carrier migration path and free radical generation mechanism of photocatalysis, piezoelectric catalysis and piezo-photocatalysis are shown in Fig. 9. When photocatalyzed alone, the E_g value of $Bi_2Fe_4O_9$ is relatively small (2.16 eV), which can capture visible light. Photon energy excites electrons from VB to CB, and photogenerated electrons e^- accumulate on CB, leaving holes h^+ on VB. Since E_{CB} of $Bi_2Fe_4O_9$ is more negative than the reduction potential of $O_2/\cdot O_2^-$ (−0.33 eV), photogenerated electrons e^- can reduce O_2 to generate active free radicals $\cdot O_2^-$ for the degradation of KN-R. At the same time, E_{VB} of

$Bi_2Fe_4O_9$ is 1.73 eV, which is more cathodic than the oxidation potential of $OH^-/\cdot OH$ (1.99 eV), so the photogenerated holes h^+ cannot oxidize OH^- to generate $\cdot OH$, but directly oxidize KN-R. In the piezoelectric catalysis, the ESR test demonstrates the presence of $\cdot OH$. This is because the US induces the formation of a piezoelectric potential that gradually decreases through the material from the poles to the center. The piezoelectric potential causes the overall tilt of the VB position of the material[9,40], and the VB on the surface of the positive electrode of $Bi_2Fe_4O_9$ is lower than 1.99 eV, thus reducing OH^- to $\cdot OH$ for the degradation of KN-R. However, in this process, the external energy input by the US is low and the concentration of free charges is low. Under the simultaneous action of US and UL, a large amount of free charges are excited, and the trend of shielding piezoelectric potential on the volume phase transfer and interface transfer paths is more obvious. In this process, more h^+, $\cdot OH$ and $\cdot O_2^-$ can be generated for the degradation of organic matter, significantly improving the efficiency of catalytic degradation.

The piezoelectric effect of the US modulates the energy band structure of $Bi_2Fe_4O_9$ while facilitating the separation of photogenerated electron-hole pairs and increasing the concentration of reactive species, which enhances the degradation efficiency of KN-R.

The reaction equations are as follows:

$$Bi_2Fe_4O_9 \xrightarrow{US/hv} e^- + h^+, \tag{4}$$

$$OH^- + h^+ \longrightarrow \cdot OH, \tag{5}$$

$$O_2 + e^- \longrightarrow \cdot O_2^-, \tag{6}$$

$$\text{KN-R} + \cdot OH,\ h^+,\ \cdot O_2^- \longrightarrow \text{degradation products}. \tag{7}$$

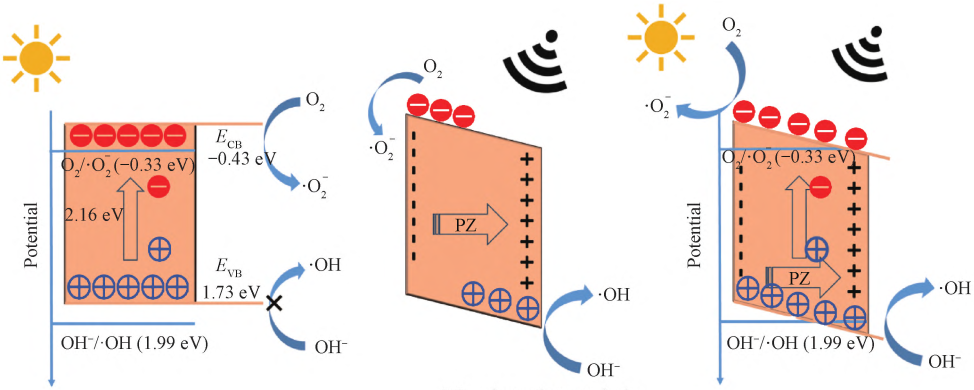

PZ—piezo-photocatalysis.

Fig. 9 Mechanism of $Bi_2Fe_4O_9$ in piezo-photocatalytic degradation of KN-R

3 Conclusions

This research focuses on the performance of $Bi_2Fe_4O_9$ in piezo-photocatalytic degradation of KN-R. The degradation efficiency of KN-R can be significantly improved by piezo-photocatalysis, and the degradation rate constant $k_{pi\text{-}ph}$ is about 3.4 times as large as k_{pi} and about 2.6 times as large as k_{ph}. The pH value of 3 and the lower KN-R mass concentration (60 mg/L) result in better degradation efficiency (98.5%). CO_3^{2-} and cationic surfactant CTAB inhibit the degradation of KN-R. It is proved that the contributions of different active species to the degradation of KN-R follow the order: $\cdot OH$, $\cdot O_2^-$, h^+, and $^1O_2$. The possible mechanism of $Bi_2Fe_4O_9$ in piezo-photocatalytic degradation of KN-R is discussed: light excitation generates a large amount of free charges, the piezoelectric effect modulates the energy band structure of $Bi_2Fe_4O_9$ and promotes the separation of photogenerated electron-hole pairs, and the synergistic effect of the two factors can significantly improve the degradation efficiency of KN-R. It provides a new strategy for developing highly efficient piezo-photocatalysts and improving the efficiency of solar energy utilization.

References

[1] LAN D W, ZHU H W, ZHANG J W, et al. Adsorptive removal of organic dyes via porous materials for wastewater treatment in recent decades: a review on species, mechanisms and perspectives[J]. *Chemosphere*, 2022, 293: 133464.

[2] WANG B X, HAN X, ZHANF X Y, et al. Reactive dyeing of wool fabric using recycled dyeing wastewater[J/OL]. *Journal of Donghua University (English Edition)*, (2024-12-17)[2024-12-25]. https://doi.org/10.19884/j.1672-5220.202406014.

[3] PRAKRUTHI K, UJWAL M P, YASHAS S R, et al. Recent advances in photocatalytic remediation of emerging organic pollutants using semiconducting metal oxides: an overview[J]. *Environmental Science and Pollution Research*, 2022, 29(4): 4930-4957.

[4] PUDLÁK M, PINČÁK R. Photosynthetic complex: exciton transfer and electron-hole separation quantum yields [J]. *The Journal of Physical Chemistry A*, 2023, 127(28): 5795-5804.

[5] WANG X X, LI L Y, FU Z, et al. Carbon quantum dots decorated CuS nanocomposite for effective degradation of methylene blue and antibacterial performance [J]. *Journal of Molecular Liquids*, 2018, 268: 578-586.

[6] RIENTE P, FIANCHINI M, LLANES P, et al. Shedding light on the nature of the catalytically active species in photocatalytic reactions using Bi_2O_3 semiconductor [J]. *Nature Communications*, 2021, 12: 625.

[7] STARR M B, SHI J, WANG X D. Piezopotential-driven redox reactions at the surface of piezoelectric materials [J]. *Angewandte Chemie International Edition*, 2012, 51(24): 5962-5966.

[8] LI H D, SANG Y H, CHANG S J, et al. Enhanced ferroelectric-nanocrystal-based hybrid photocatalysis by ultrasonic-wave-generated piezophototronic effect[J]. *Nano Letters*, 2015, 15(4): 2372-2379.

[9] WU J, QIN N, BAO D H. Effective enhancement of piezocatalytic activity of $BaTiO_3$ nanowires under ultrasonic vibration [J]. *Nano Energy*, 2018, 45: 44-51.

[10] LIU Y L, WU J M. Synergistically catalytic activities of $BiFeO_3/TiO_2$ core-shell nanocomposites for degradation of organic dye molecule through piezophototronic effect [J]. *Nano Energy*, 2019, 56: 74-81.

[11] YUAN J, HUANG X Y, ZHANG L L, et al. Tuning piezoelectric field for optimizing the coupling effect of piezo-photocatalysis [J]. *Applied Catalysis B: Environmental*, 2020, 278: 119291.

[12] LAN S Y, YU C, SUN F, et al. Tuning piezoelectric driven photocatalysis by La-doped magnetic $BiFeO_3$-based multiferroics for water purification[J]. *Nano Energy*, 2022, 93: 106792.

[13] HONG K S, XU H F, KONISHI H, et al. Direct water splitting through vibrating piezoelectric microfibers in water[J]. *The Journal of Physical Chemistry Letters*, 2010, 1(6): 997-1002.

[14] HONG K S, XU H F, KONISHI H, et al. Piezoelectrochemical effect: a new mechanism for azo dye decolorization in aqueous solution through vibrating piezoelectric microfibers [J]. *The Journal of Physical Chemistry C*, 2012, 116 (24): 13045-13051.

[15] LIN J H, TSAO Y H, WU M H, et al. Single- and few-layers MoS_2 nanocomposite as piezo-catalyst in dark and self-powered active sensor [J]. *Nano Energy*, 2017, 31: 575-581.

[16] WU J M, CHANG W E, CHANG Y T, et al. Piezo-catalytic effect on the enhancement of the ultra-high degradation activity in the dark by single- and few-layers MoS_2 nanoflowers [J]. *Advanced Materials*, 2016, 28(19): 3718-3725.

[17] XU X L, JIA Y M, XIAO L B, et al. Strong vibration-catalysis of ZnO nanorods for dye wastewater decolorization via piezo-electro-chemical coupling [J]. *Chemosphere*, 2018, 193: 1143-1148.

[18] DU Y M, LU T, LI X N, et al. High-efficient piezocatalytic hydrogen evolution by centrosymmetric $Bi_2Fe_4O_9$ nanoplates [J]. *Nano Energy*, 2022, 104: 107919.

[19] TIAN Z M, QIU Y, YUAN S L, et al. Enhanced multiferroic properties in Ti-doped $Bi_2Fe_4O_9$ ceramics [J]. *Journal of Applied Physics*, 2010, 108(6): 64110.

[20] YIN S M, LI W Q, CHENG R S, et al. Hydrothermal synthesis, photocatalytic and magnetic properties of pure-phase $Bi_2Fe_4O_9$ microstructures [J]. *Journal of Electronic Materials*, 2021, 50(3): 954-959.

[21] MA M L, CHEN Y, LIU Y Y, et al. Highly efficient photocatalytic organic dyes degradation based on 1D magnetic $Bi_2Fe_4O_9$/C @ AgBr composite[J]. *Applied Organometallic Chemistry*, 2022, 36(5): e6619.

[22] WANG Y, TANG Y R, SUN J H, et al. $BiFeO_3/Bi_2Fe_4O_9$ S-scheme heterojunction hollow nanospheres for high-efficiency photocatalytic *o*-chlorophenol degradation[J]. *Applied Catalysis B: Environmental*, 2022, 319: 121893.

[23] WU T L, LIU L, PI M Y, et al. Enhanced magnetic and photocatalytic properties of $Bi_2Fe_4O_9$ semiconductor with large exposed (001) surface [J]. *Applied Surface Science*, 2016, 377: 253-261.

[24] SU C J, LI C L, LI R H, et al. Insights into highly efficient piezocatalytic molecule oxygen activation over $Bi_2Fe_4O_9$: active sites and mechanism[J]. *Chemical Engineering Journal*, 2023, 452: 139300.

[25] XU G R, WANG J, ZHANG N, et al. Ferroelectric polarization promoted electrocatalytic hydrogen evolution on $Bi_2Fe_4O_9$ nanoplates [J]. *Scripta Materialia*, 2023, 232: 115509.

[26] ZHANG Y Y, ZHOU C Y, LONG H M, et al. Efficient oxidation of ibuprofen by nano-plate $Bi_2Fe_4O_9$ activated peroxymonosulfate [J]. *Separation and Purification Technology*, 2023, 319: 124044.

[27] OH W D, CHANG V W C, LIM T T. A comprehensive performance evaluation of heterogeneous $Bi_2Fe_4O_9$/peroxymonosulfate system for sulfamethoxazole degradation [J]. *Environmental Science and Pollution Research*,

2019, 26(2): 1026-1035.

[28] LIU H H, LI L, GUO C F, et al. Thickness-dependent carrier separation in $Bi_2Fe_4O_9$ nanoplates with enhanced photocatalytic water oxidation [J]. *Chemical Engineering Journal*, 2020, 385: 123929.

[29] DU Y, CHENG Z X, DOU S X, et al. Effect of chromium substitution on structure and magnetic properties of $Bi_2Fe_4O_9$ [J]. *Materials Letters*, 2010, 64(20): 2251-2254.

[30] KIRSCH A, MURSHED M M, SCHOWALTER M, et al. Nanoparticle precursor into polycrystalline $Bi_2Fe_4O_9$: an evolutionary investigation of structural, morphological, optical, and vibrational properties [J]. *The Journal of Physical Chemistry C*, 2016, 120(33): 18831-18840.

[31] WANG K, LI Y, ZHANG G K, et al. 0D Bi nanodots/2D Bi_3NbO_7 nanosheets heterojunctions for efficient visible light photocatalytic degradation of antibiotics: enhanced molecular oxygen activation and mechanism insight [J]. *Applied Catalysis B: Environmental*, 2019, 240: 39-49.

[32] BIESINGER M C, PAYNE B P, GROSVENOR A P, et al. Resolving surface chemical states in XPS analysis of first row transition metals, oxides and hydroxides: Cr, Mn, Fe, Co and Ni [J]. *Applied Surface Science*, 2011, 257(7): 2717-2730.

[33] TAN C Q, GAO N Y, FU D F, et al. Efficient degradation of paracetamol with nanoscaled magnetic $CoFe_2O_4$ and $MnFe_2O_4$ as a heterogeneous catalyst of peroxymonosulfate [J]. *Separation and Purification Technology*, 2017, 175: 47-57.

[34] ZHU Q H, HAILILI R, XIN Y, et al. Efficient full spectrum responsive photocatalytic NO conversion at $Bi_2Ti_2O_7$: co-effect of plasmonic Bi and oxygen vacancies [J]. *Applied Catalysis B: Environmental*, 2022, 319: 121888.

[35] ZHANG J Y, ZHU G Q, LI S P, et al. Novel Au/La-Bi_5O_7I microspheres with efficient visible-light photocatalytic activity for NO removal: synergistic effect of Au nanoparticles, La doping, and oxygen vacancy [J]. *ACS Applied Materials & Interfaces*, 2019, 11(41): 37822-37832.

[36] TU S C, ZHANG Y H, RESHAK A H, et al. Ferroelectric polarization promoted bulk charge separation for highly efficient CO_2 photoreduction of $SrBi_4Ti_4O_{15}$ [J]. *Nano Energy*, 2019, 56: 840-850.

[37] LIANG Z Q, BAI X J, HAO P, et al. Full solar spectrum photocatalytic oxygen evolution by carbon-coated TiO_2 hierarchical nanotubes [J]. *Applied Catalysis B: Environmental*, 2019, 243: 711-720.

[38] ZHANG N, JALIL A, WU D X, et al. Refining defect states in $W_{18}O_{49}$ by Mo doping: a strategy for tuning N_2 activation towards solar-driven nitrogen fixation [J]. *Journal of the American Chemical Society*, 2018, 140(30): 9434-9443.

[39] WANG S B, GUAN B Y, WANG X, et al. Formation of hierarchical Co_9S_8 @ $ZnIn_2S_4$ heterostructured cages as an efficient photocatalyst for hydrogen evolution [J]. *Journal of the American Chemical Society*, 2018, 140(45): 15145-15148.

[40] SU R, HSAIN H A, WU M, et al. Nano-ferroelectric for high efficiency overall water splitting under ultrasonic vibration [J]. *Angewandte Chemie International Edition*, 2019, 58(42): 15076-15081.

基于铁酸铋（$Bi_2Fe_4O_9$）的压电光催化技术降解活性染料 KN-R

朱飞狮[1, 2]，胡春艳[1, 2]，刘保江[1, 2*]
1. 东华大学 生态纺织教育部重点实验室，上海 201620
2. 东华大学 化学与化工学院，上海 201620

摘　要：印染废水对环境保护和工业发展构成严重威胁。压电效应可以用来优化半导体的能带结构，提高光催化剂的光子效率。该研究采用水热合成方法制备了具有压电效应的窄间隙半导体 $Bi_2Fe_4O_9$，用于降解染色废水中的活性染料 KN-R。研究结果表明，$Bi_2Fe_4O_9$ 压电光催化能够显著提高降解 KN-R 的效率。压电光催化降解速率常数 $k_{pi\text{-}ph}$ 分别约为压电催化降解速率常数 k_{pi} 和光催化降解速率常数 k_{ph} 的 3.4 倍和 2.6 倍。当 pH 值为 3 且 KN-R 质量浓度较低（60 mg/L）时，降解效率高（98.5%）。CO_3^{2-} 和阳离子表面活性剂（CTAB）会抑制 KN-R 的降解。活性物种类对降解 KN-R 的贡献程度依次为：$\cdot OH$，$\cdot O_2^-$，h^+，$^1O_2$。可能的压电光催化降解机理为光激发产生大量的自由电荷，压电效应调节了 $Bi_2Fe_4O_9$ 的能带结构并促进了光生电子空穴对的分离，两者协同作用显著提高了 KN-R 的降解效率。

关键词：$Bi_2Fe_4O_9$；压电光催化；降解；废水处理；活性染料 KN-R